Supporting Information

Breaking the Limits of Ruddlesden-Popper Cathodes to Achieve a Game-Changer for Proton-Conducting Solid Oxide Fuel Cells

Yanru Yin [a], Hongfang Huang [a], Samir Boulfrad [b], Hailu Dai [c], Yueyuan Gu [a], Shoufu Yu [a] and Lei Bi [a, *]

a. School of Resource Environment and Safety Engineering, University of South China, Hengyang 421001, China

b. College of Science & Engineering, Hamad Bin Khalifa University, Doha 34110, Qatar

c. School of Materials Science and Engineering, Yancheng Institute of Technology, Yancheng 224051, China

*Corresponding author

Email: lei.bi@usc.edu.cn, bilei81@gmail.com

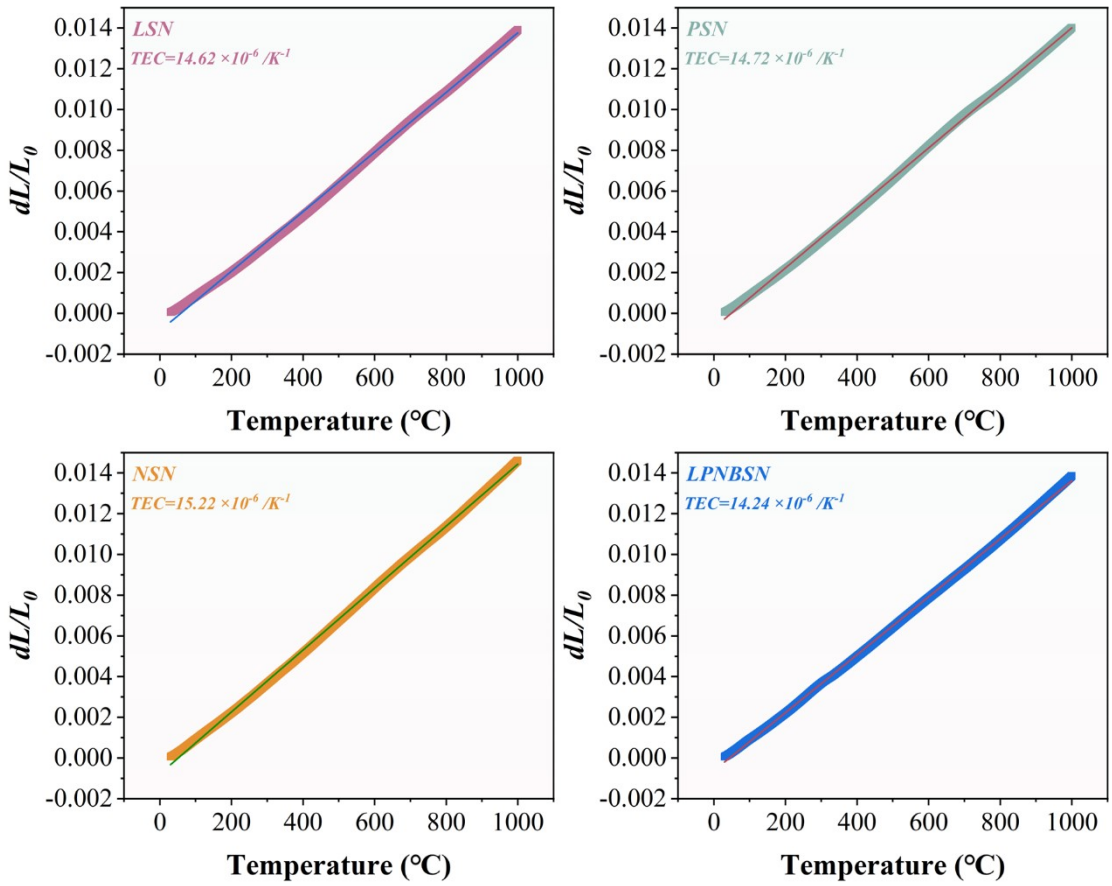

Figure S1. TEC curves for LSN, PSN, NSN and LPNBSN.

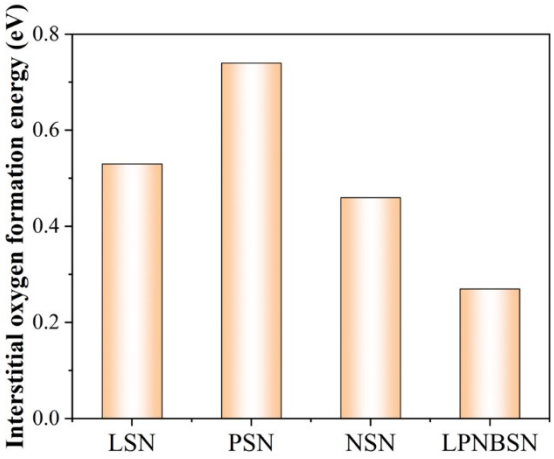

Figure S2. Interstitial oxygen formation energy for LSN, PSN, NSN and LPNBSN.

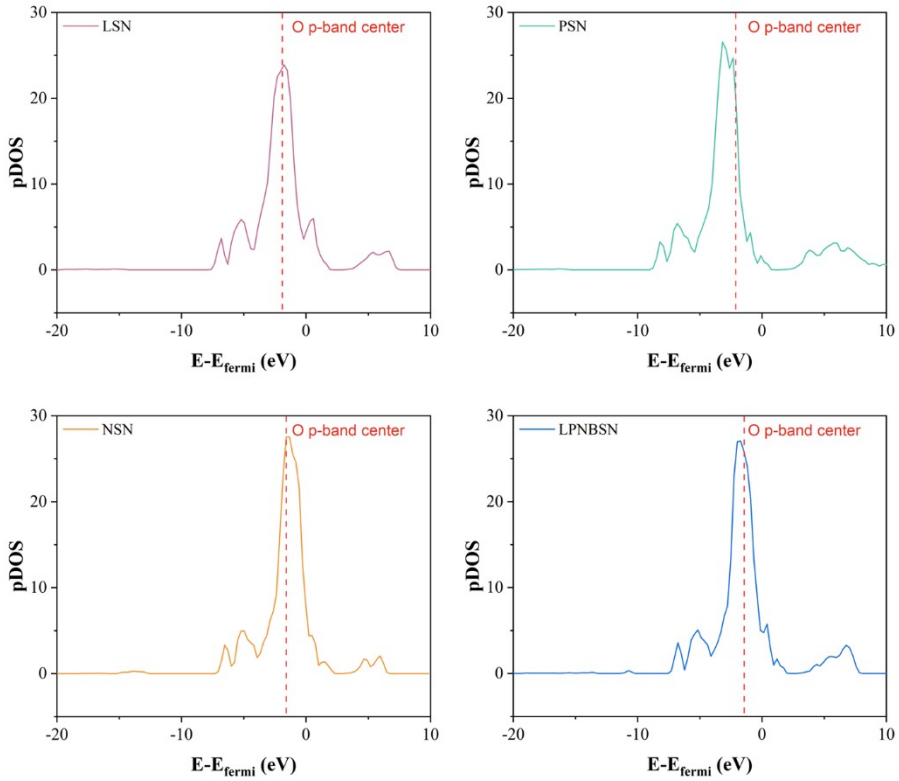

Figure S3. O p-DOS for LSN, PSN, NSN and LPNBSN.

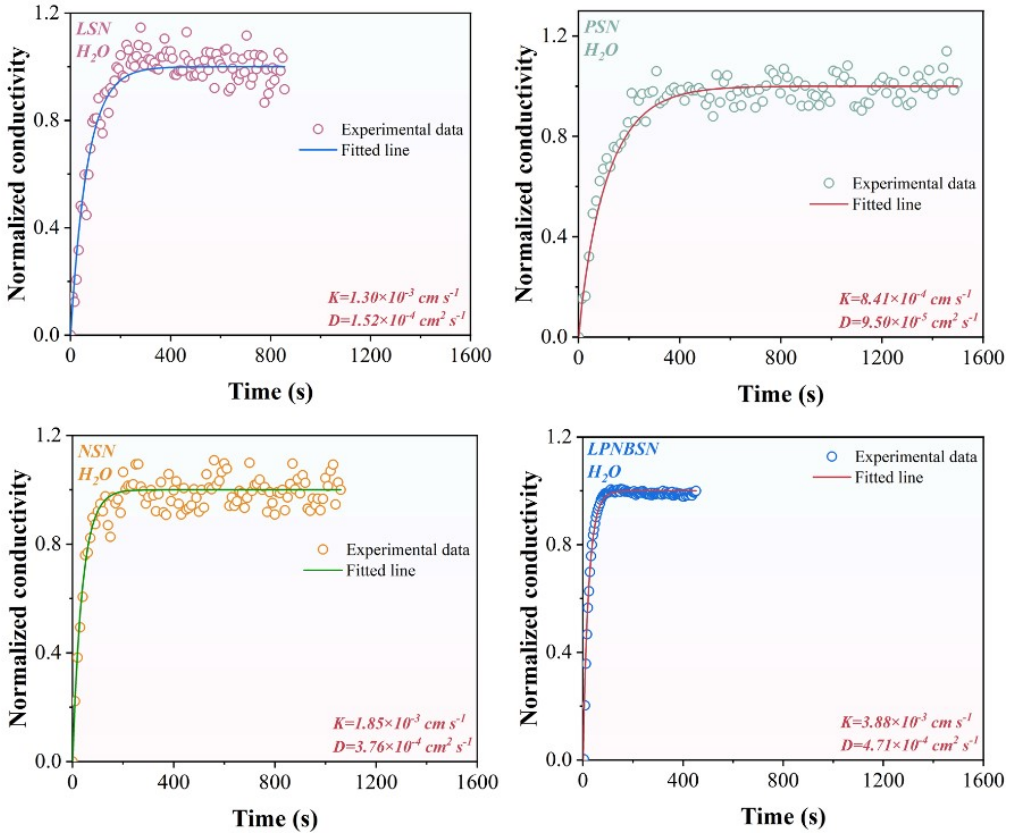

Figure S4. ECR curves for LSN, PSN, NSN and LPNBSN measured at 600 °C by abruptly changing the testing condition from dry to wet air.

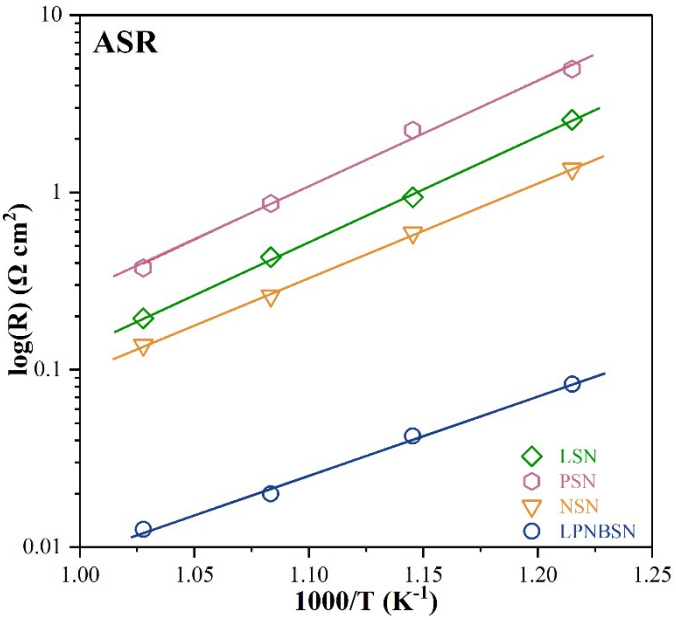

Figure S5. ASR of LSN, PSN, NSN and LPNBSN cathodes obtained from symmetrical cell measurements tested under a wet air condition.

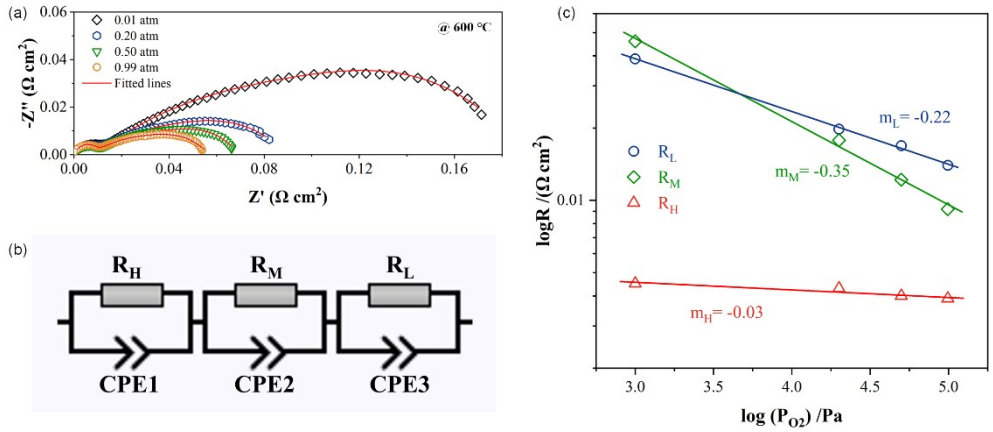

Figure S6. (a) EIS plots of LPNBSN symmetrical cell is tested under different oxygen partial pressures and (b) the equivalent circuit used to fit the EIS plot. (c) R_H, R_M and R_L as a function of pO_2 tested at 600 ^oC.

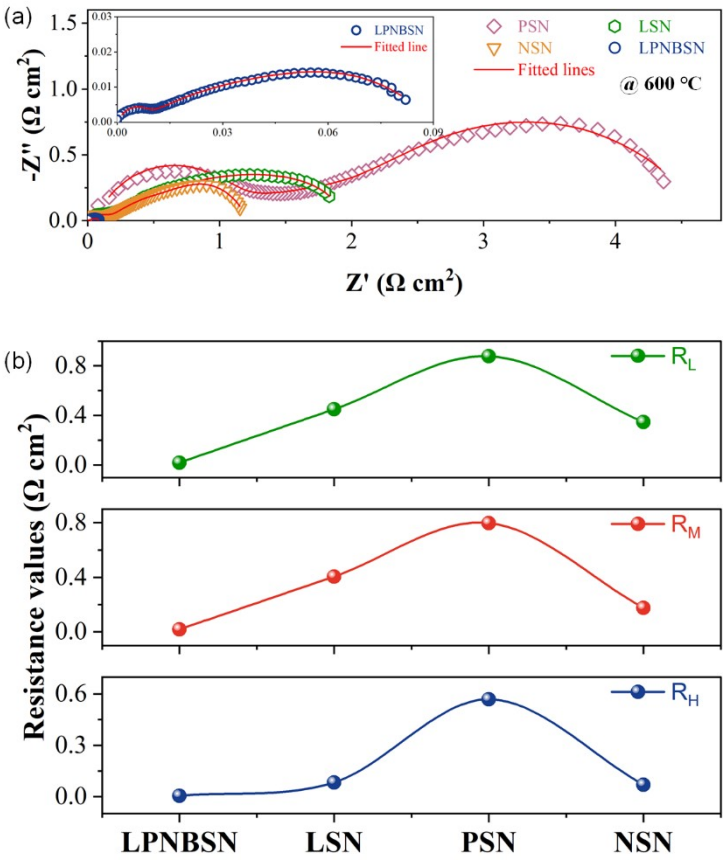

Figure S7. (a) EIS plots for LSN, PSN, NSN, LPNBSN symmetrical cells tested at 600 °C and (b) their corresponding R_H, R_M and R_L.

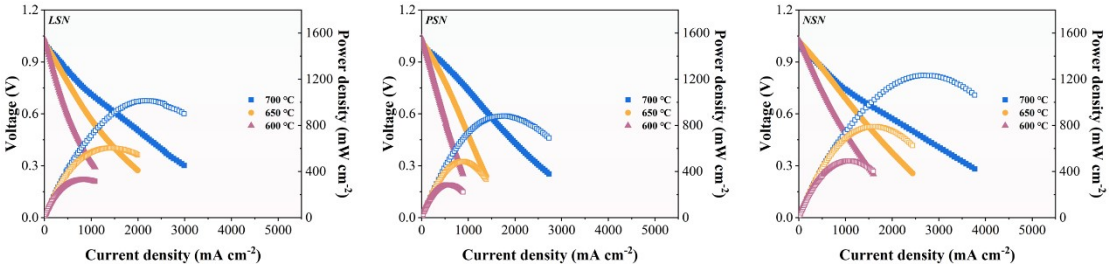

Figure S8. Performance of H-SOFCs using LSN, PSN and NSN cathodes.

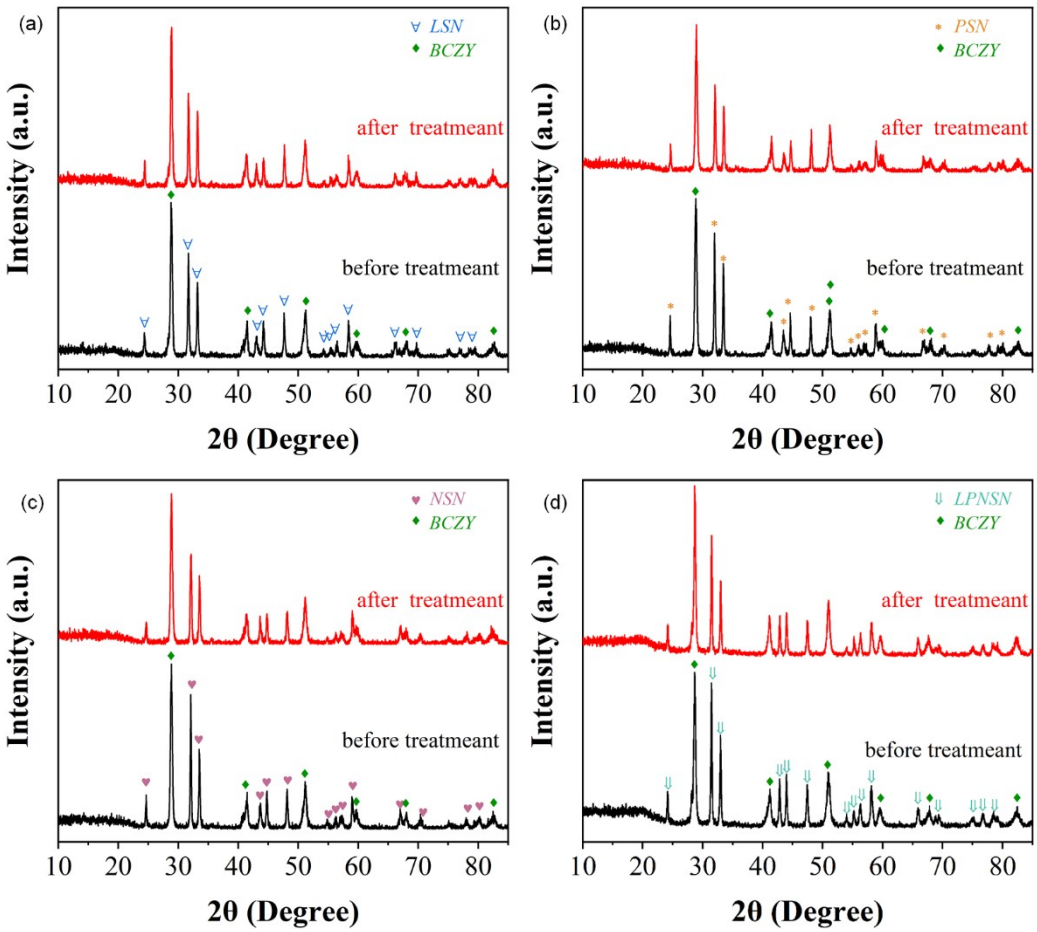

Figure S9. XRD patterns for LSN+BCZY, PSN+BCZY, NSN+BCZY and LPNBSN+BCZY before and after co-firing at 900 °C for 2 h.

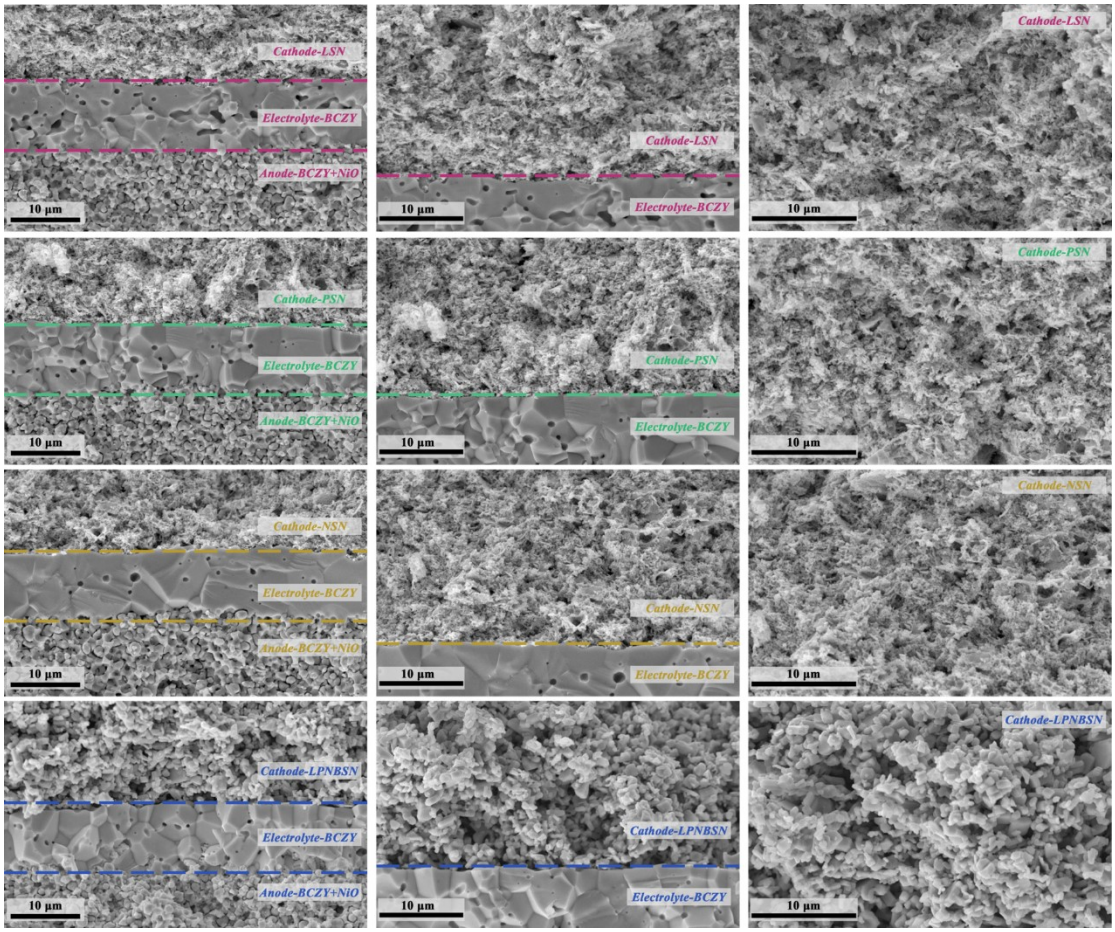

Figure S10. Cross-sectional views for the fuel cells using LSN, PSN, NSN and LPNBSN cathodes.

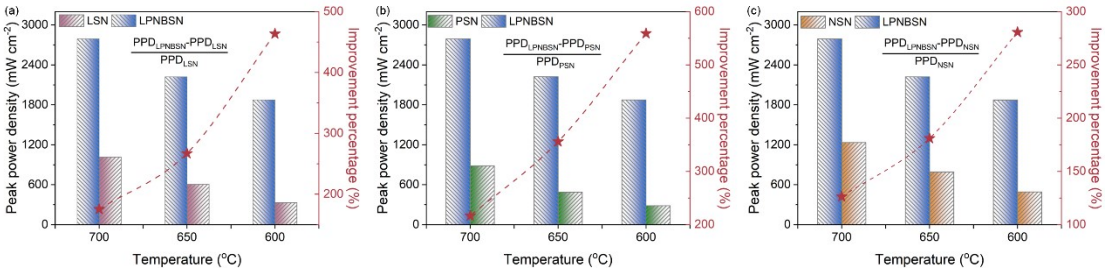

Figure S11. PPD comparison and increment percentage between the cells using (a) LSN and LPNBSN, (b) PSN and LPNBSN, (c) NSN and LPNBSN cathodes at different temperatures.

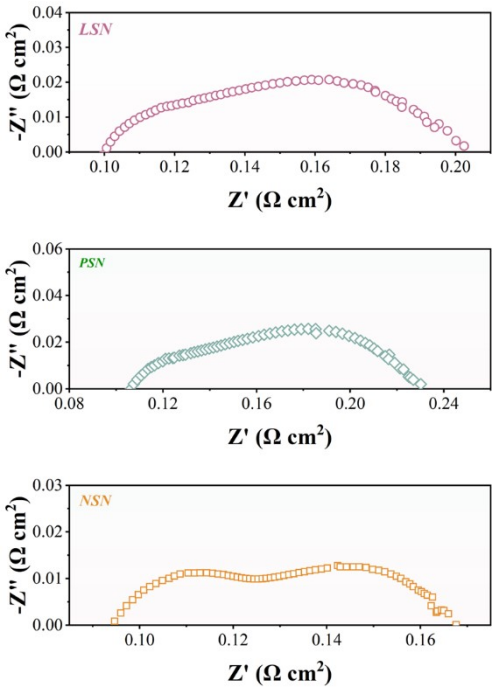

Figure S12. EIS plots for the cells using LSN, PSN, NSN cathodes measured at 700 ^{o}C.

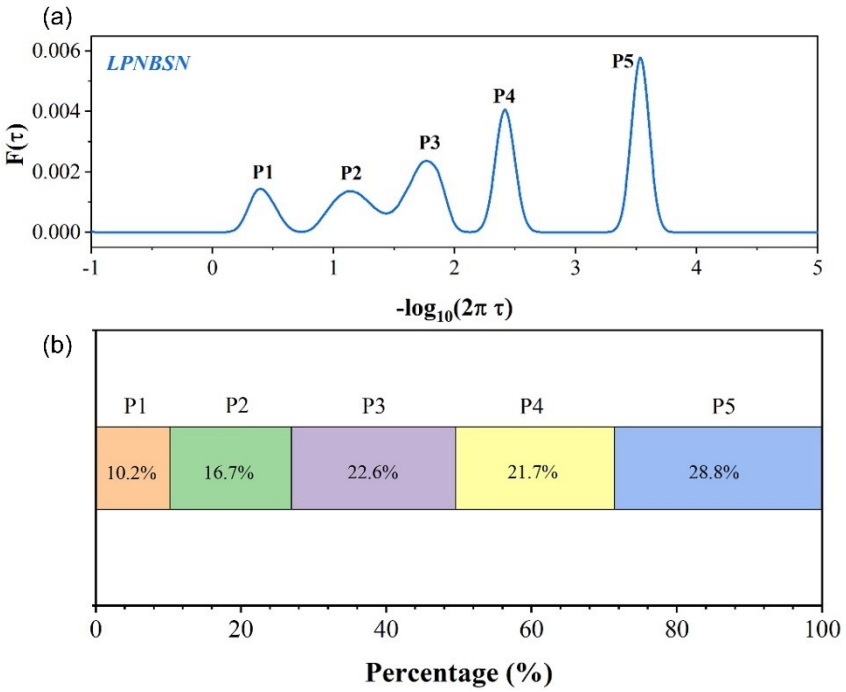

Figure S13. (a) DRT plot for the LPNBSN cell at tested 700 °C and (b) the portion of each peak.

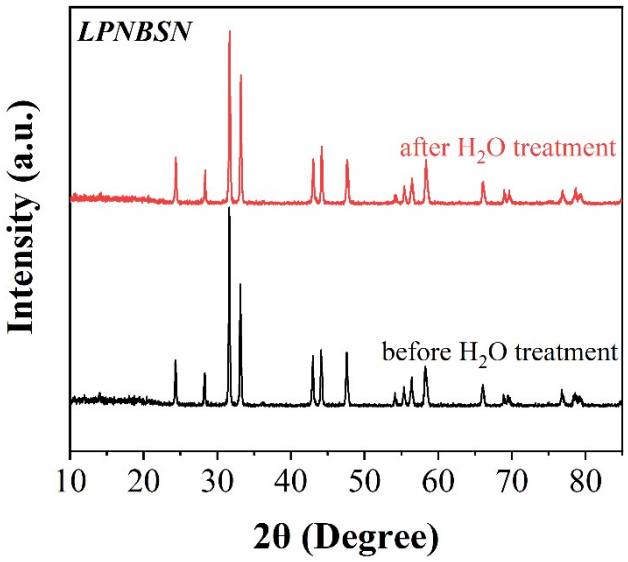

Figure S14. XRD patterns for LPNBSN before and after the treatment in a 30% H_2O-containing atmosphere at 600 °C for 10 h.

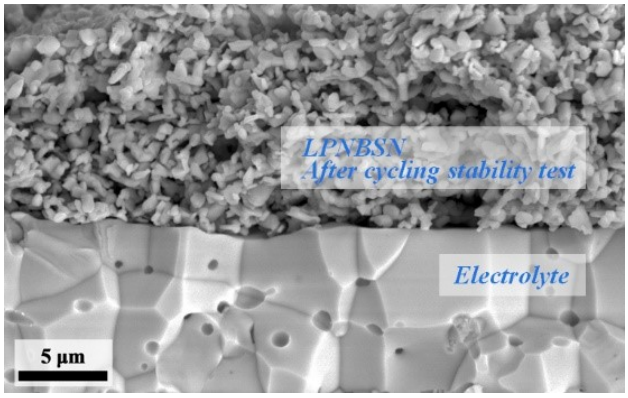

Figure S15. SEM image for the LPNBSN cathode and electrolyte interface after the cycling test.

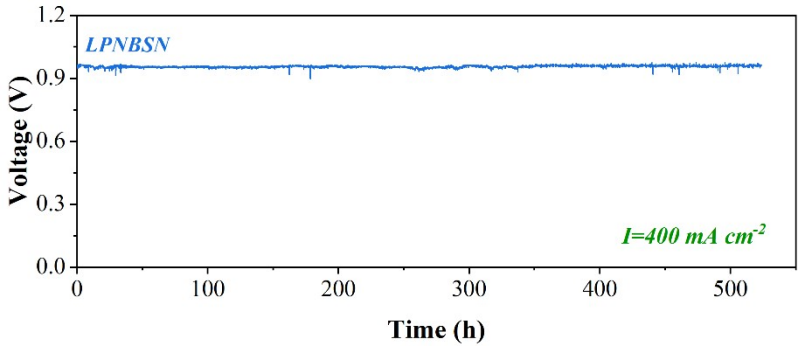

Figure R16. Operational stability of an H-SOFC using the LPNBSN cathode under the fuel cell working condition at 600 ^{o}C for more than 500 hours.

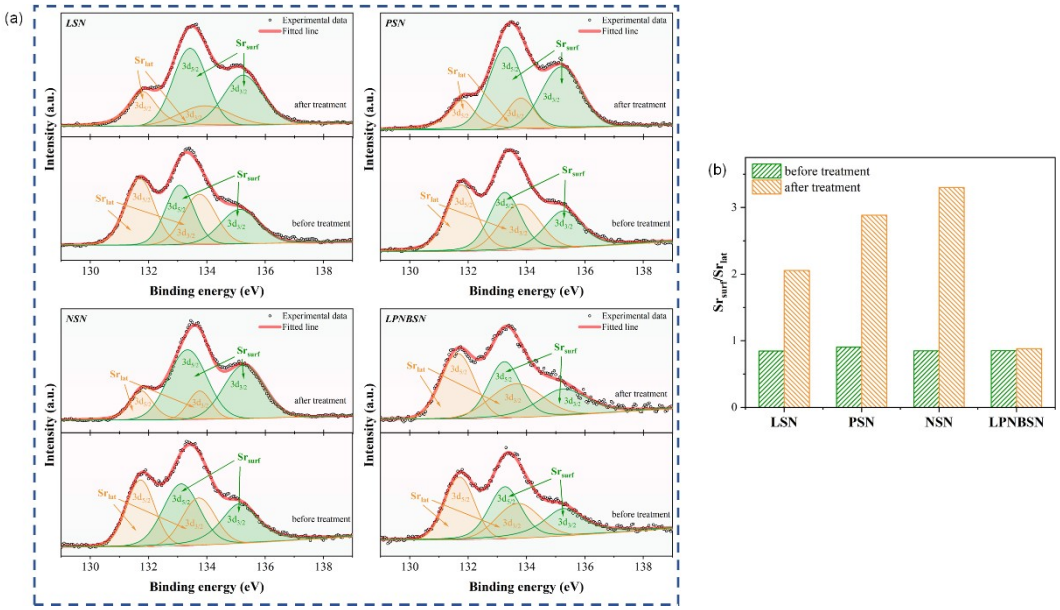

Figure S17. (a) XPS Sr 3d spectra and (b) the proportion of surface Sr to lattice Sr for LSN, PSN, NSN and LPNBSN before and after the thermal treatment.

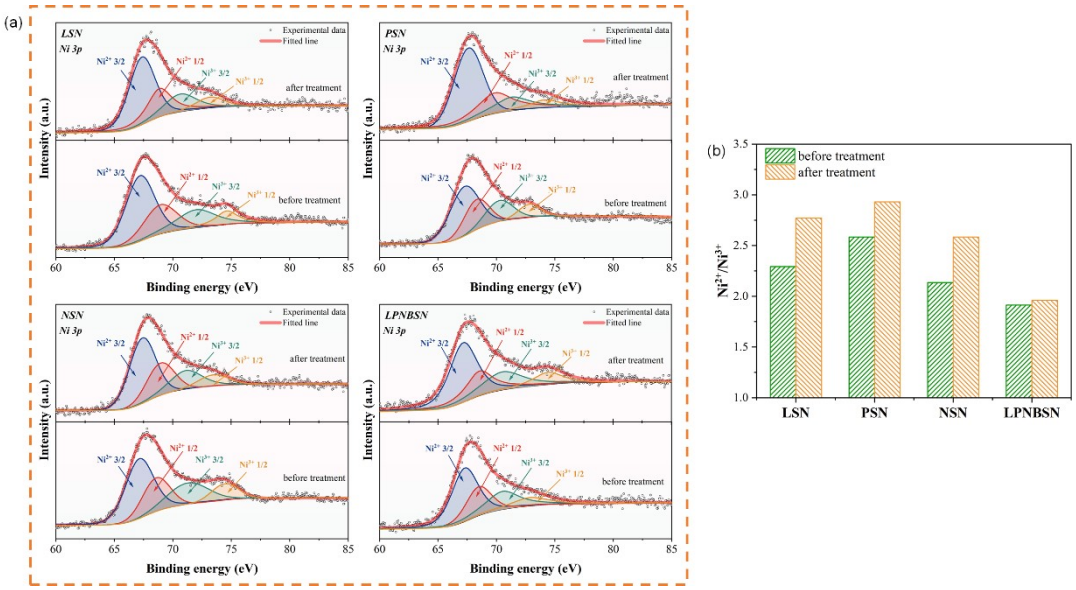

Figure S18. (a) XPS Ni 3p spectra and (b) the Ni^{2+}/Ni^{3+} ratio for LSN, PSN, NSN and LPNBSN before and after the thermal treatment.

Table S1. D_h and k_h values for LSN, PSN, NSN and LPNBSN measured at 600 °C.

	LSN	PSN	NSN	LPNBSN
$D_h/\times10^{-4}$ cm^2 s^{-1}	1.52	0.95	3.76	4.71
$k_h/\times10^{-3}$ cm s^{-1}	1.30	0.84	1.85	3.88